# Spectra of Rg-water dimers in the region of the $D_2O$ $\nu_3$ asymmetric stretch (Rg = Ar, Kr, Xe)

R. Glorieux,[1] A. J. Barclay,[2] C. Lauzin,[1] A. R. W. McKellar,[3] and N. Moazzen-Ahmadi[2*]

[1]*Institute of Condensed Matter and Nanosciences, Université catholique de Louvain (U.C.L.), Chemin du cyclotron 2, 1348 Louvain-la-Neuve, Belgium*
[2]*Department of Physics and Astronomy, University of Calgary, 2500 University Drive North West, Calgary, Alberta T2N 1N4, Canada*
[3]*National Research Council of Canada, Ottawa, Ontario K1A 0R6, Canada*

**Abstract**

Spectra of rare gas (Rg) – $D_2O$ dimers (Rg = Ar, Kr, Xe) are studied in the region of the $D_2O$ $\nu_3$ asymmetric stretch (≈2800 $cm^{-1}$), using a rapid-scan tunable infrared optical parametric oscillator source to probe a pulsed supersonic slit jet expansion. Three bands are observed in each case, labeled according to the $D_2O$ rotational transition with which they correlate as: $\Sigma(1_{01}) \leftarrow \Sigma(0_{00})$, $\Pi(1_{01}) \leftarrow \Sigma(0_{00})$, and $\Sigma(0_{00}) \leftarrow \Sigma(1_{01})$. The Ar-$D_2O$ bands exhibit various perturbations and line broadening effects. For Kr-$D_2O$, the $\Pi(1_{01}) \leftarrow \Sigma(0_{00})$ and $\Sigma(0_{00}) \leftarrow \Sigma(1_{01})$ bands are simple and relatively unperturbed with almost no resolved Kr isotope structure, while the $\Sigma(1_{01}) \leftarrow \Sigma(0_{00})$ band is highly perturbed and shows large isotope splittings. This latter perturbation is analyzed in detail with good results. For Xe-$D_2O$, the experimental spectra are unfortunately weaker. Analysis of the $\Pi(1_{01}) \leftarrow \Sigma(0_{00})$ and $\Sigma(0_{00}) \leftarrow \Sigma(1_{01})$ bands is again relatively straightforward, but the $\Sigma(1_{01}) \leftarrow \Sigma(0_{00})$ band is even more perturbed than for Kr-$D_2O$ and its analysis proves impossible. Line broadening (for Ar-$D_2O$) and vibrational frequency shift effects are described.

*Corresponding author: N. Moazzen-Ahmadi
Email: nmoazzen@ucalgary.ca

## 1. Introduction

Rare gas (Rg) - water dimers are the simplest of the many possible weakly-bound clusters containing the water molecule, but their detailed understanding still poses interesting challenges. Beginning in 1988 with far-infrared spectroscopy of Ar-$H_2O$ by Cohen et al.,[1] there have been over forty Rg-water publications, counting only high-resolution (gas-phase) spectra and closely related theory. Almost half of these have appeared in the last ten years.

Theoretical equilibrium structures for Rg-water, given by the minimum of the potential energy surface, generally locate the Rg atom in the plane of the water molecule with an approximately hydrogen-bonded configuration adjacent to an H (or D) atom.[2] But the energy barriers for rotation of the water molecule are relatively low, especially when water's small rotational moments of inertia are taken into consideration, so that it is fairly free to rotate relative to the Rg atom. For this reason, most studies have analyzed Rg-water not in terms of an asymmetric rotor molecule (which it is), but rather in terms of a pseudo-diatomic molecule with different "vibrational" states, each of which correlates with a particular water monomer rotational state. Thus the ground state of Rg-water corresponds to the $J_{KaKc} = 0_{00}$ level of water, and excited states correspond to rotational levels $1_{01}$, $1_{11}$, $1_{10}$, $2_{02}$, etc. When $J > 0$, it is necessary to specify its projection on the intermolecular axis, so the Rg-water states have labels like $\Sigma(0_{00})$, $\Sigma(1_{01})$, $\Pi(1_{01})$, $\Sigma(1_{11})$, etc., with $\Sigma$, $\Pi$, $\Delta$…, denoting projections of 0, 1, 2…. Of course we know that $H_2O$ and $D_2O$ have distinct nuclear spin species, one with ($K_a$, $K_c$) = (even, even) or (odd, odd), and the other with (even, odd) or (odd, even), in the ground vibrational state. This carries over into Rg-water, so that if spin relaxation is slow, then even at very low temperatures (≈2 K in the present work) there are two populated "ground" states, $\Sigma(0_{00})$ and either $\Sigma(1_{01})$ or $\Pi(1_{01})$ depending on which is lower in energy. For $D_2O$, as studied here, the $0_{00}$ level belongs to the *ortho* species with a spin weight of 6, and the $1_{01}$ level (at an energy of 12.12 $cm^{-1}$) belongs to the *para* species with a weight of 3.

Here we describe a few previous studies which are most relevant to the present work. Spectra of Ar-$D_2O$ were first reported in 1991 by three groups: Fraser et al.[3] studied pure rotational microwave transitions within the $\Sigma(0_{00})$ and $\Sigma(1_{01})$ states, Suzuki et al.[4] studied far infrared transitions from the $\Sigma(0_{00})$ state to the $\Pi(1_{11})$ and $\Sigma(1_{11})$ states (at about 19.3 and 20.7 $cm^{-1}$, respectively), and Zwart and Meerts[5] studied far infrared transitions from the $\Sigma(1_{01})$ state to

the $\Pi(1_{01})$ and $\Pi(1_{10})$ states (at about 11.0 and 14.0 $cm^{-1}$, respectively). More recently, infrared spectra of Ar-$D_2O$ have been studied for the $D_2O$ ($\nu_1$, $\nu_2$, $\nu_3$) = (0,1,0) bending fundamental (≈1200 $cm^{-1}$)[6,7,8] and the (1,1,1) combination (≈6550 $cm^{-1}$).[9] A fairly recent theoretical publication[10] on Ar-$D_2O$ reported a new potential energy surface and focused particularly on the $D_2O$ $\nu_2$ mode. Results for Kr and Xe are more limited. Detailed microwave studies were reported for Kr-$D_2O$ by Van Wijngaarden and Jäger[11] and for Xe-$D_2O$ by Wen and Jäger,[12] with the latter also including *ab initio* potential energy surface calculations. For Kr-$D_2O$, infrared spectra have been studied in the (0,1,0) region[6] and a potential surface calculation was reported.[13]

In the present paper, we report Rg-$D_2O$ spectra in the region of the $D_2O$ $\nu_3$ fundamental (≈2800 $cm^{-1}$), including three bands in each case: $\Sigma(1_{01}) \leftarrow \Sigma(0_{00})$, $\Pi(1_{01}) \leftarrow \Sigma(0_{00})$, and $\Sigma(0_{00}) \leftarrow \Sigma(1_{01})$. Analysis of the spectra yields band origins, vibrational shifts, and upper state rotational parameters. Various perturbations and line broadening effects are observed. Especially notable is the $\Sigma(1_{01}) \leftarrow \Sigma(0_{00})$ band of Kr-$D_2O$, where a local perturbation causes large Kr isotopic splittings which we analyze in detail. For Ar-$D_2O$, transitions in this same band are broadened but otherwise relatively unperturbed, while for Xe-$D_2O$ this band is so perturbed as to resist rotational assignment. Further interesting perturbations are observed in the other two bands.

## 2. Results

Spectra were recorded as described previously[14,15] using a pulsed supersonic slit jet expansion probed by a rapid-scan tunable infrared optical parametric oscillator source. The usual supersonic expansion mixtures contained about 0.01% $D_2O$ plus 0.7% Ar, Kr, or Xe in helium carrier gas with a backing pressure of about 10 atmospheres. Wavenumber calibration was carried out by simultaneously recording signals from a fixed etalon and a room temperature reference gas cell. Spectral assignment, simulation, and fitting were made with the help of PGOPHER.[16]

### 2.1. Ar-$D_2O$

Observed spectra of Ar-$D_2O$ are illustrated in Fig. 1 for the bands $\Sigma(1_{01}) \leftarrow \Sigma(0_{00})$ and $\Sigma(0_{00}) \leftarrow \Sigma(1_{01})$, with two sets of experimental conditions yielding effective rotational temperatures of approximately 4 K (top traces) and 2 K (middle traces). The bottom traces are simulated spectra for 4 K. These simple parallel bands are analyzed as diatomic molecule $\Sigma \leftarrow \Sigma$

transitions with ground state parameters fixed at previous literature values[4,5] and the resulting parameters are listed in Table 1. A notable difference between the two bands is that all transitions in the $\Sigma(1_{01}) \leftarrow \Sigma(0_{00})$ band at 2792 $cm^{-1}$ show excess broadening due to finite upper state lifetimes (predissociation), while those in the $\Sigma(0_{00}) \leftarrow \Sigma(1_{01})$ band at 2781 $cm^{-1}$ remain sharp (limited by experimental effects) for $J' < 4$ and then broaden somewhat for $J' = 7$ to 12. These line width effects are discussed in Sec. 2.4 below. The 2792 band transitions fit very well for $J' < 9$, while the quality of the fit for the 2781 $cm^{-1}$ band is significantly worse, even though its lines are sharper. Thus the $\Sigma(0_{00})$ upper state evidently has small random perturbations for $J'$ values up to 10, whereas the $\Sigma(1_{01})$ upper state line positions are less perturbed (though broadened) up to $J' = 8$. The $\Sigma(1_{01})$ state then experiences large perturbations at $J' = 8$ and 9, after which $J' = 10$ returns to an apparently unperturbed position. We were not able to analyze these perturbations in detail.

The Ar-$D_2O$ perpendicular band $\Pi(1_{01}) \leftarrow \Sigma(0_{00})$, which is illustrated in the top panel of Fig. 2, is more perturbed than either parallel band. We are only able to assign transitions involving $J' = 1$ to 5 for the *e* parity component (i.e. the *P*- and *R*-branches) and $J' = 1$ to 4 for the *f* parity component (the *Q*-branch) because of line broadening for higher $J'$. Five adjustable parameters are used to fit eight upper state rotational levels (the broad $J' = 3e$ and $4f$ levels were not included in the fit). Due to the limited data and the presence of perturbations, the fitted parameters for the $\Pi(1_{01}) \leftarrow \Sigma(0_{00})$ band in Table 1 have large uncertainties and are not very meaningful. The simulated spectrum in Fig. 2, based on these parameters, does not agree well with the observed spectrum, in which we note strong sharp *Q*(1) and *Q*(2) lines, a somewhat weaker *Q*(3) line, and then a very broad *Q*(4). Some further broad *Q*-branch lines seem to be visible in the 4 K spectrum, but their assignment is uncertain. The *P*- and *R*-branch lines are considerably weaker than the *Q*-branch, and quickly lose peak intensity with increasing $J'$, showing large broadening for $J' = 3$. The sudden broadening of the $J' = 3e$ and $4f$ levels must be due to an interaction with a (short lifetime) perturbing state, but there is not enough information for an analysis. Line broadening is discussed further below (Sec. 2.4).

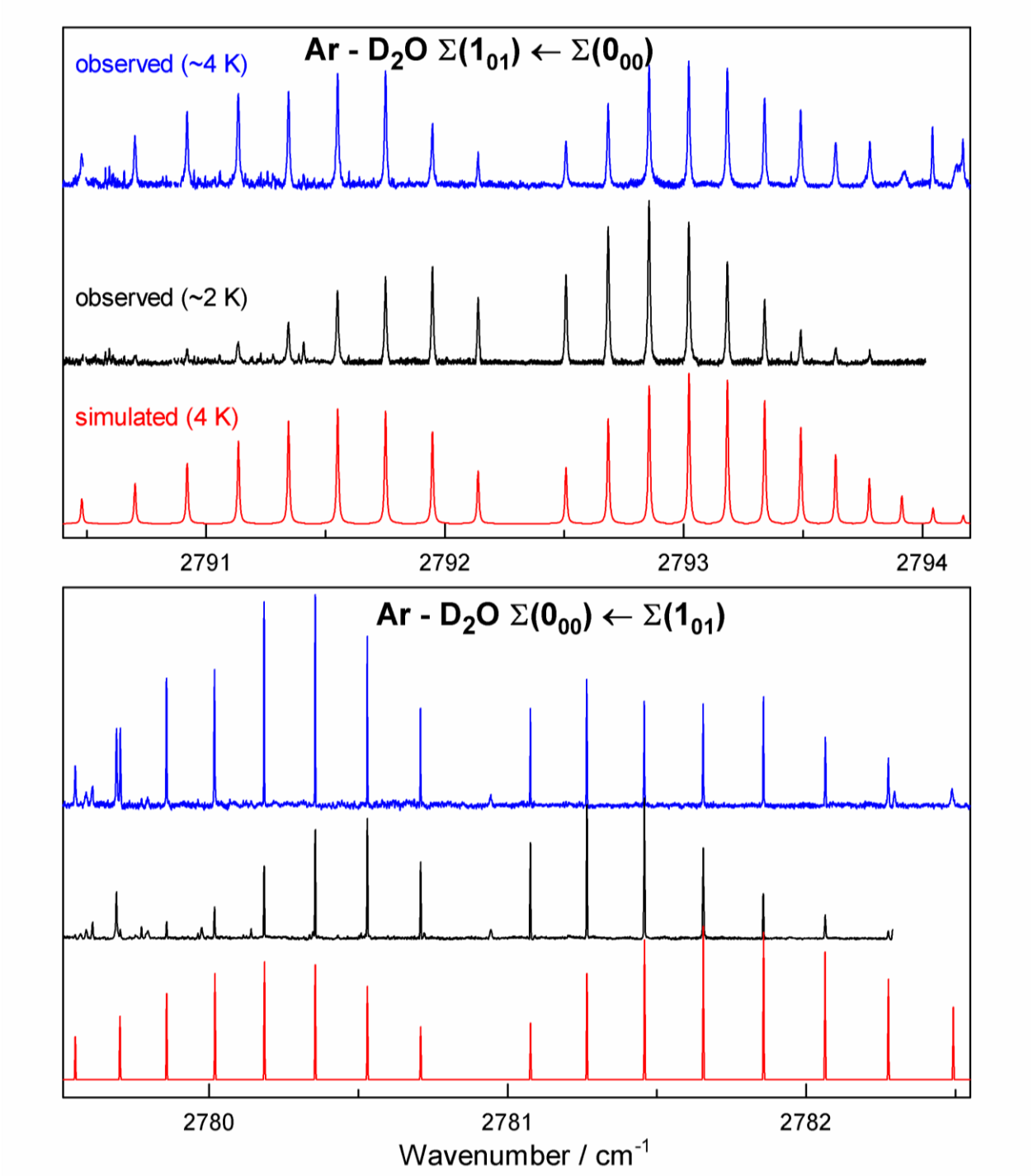


Figure 1. Observed and simulated spectra of Ar-$D_2O$. The FWHM of the lines in the $\Sigma(1_{01}) \leftarrow \Sigma(0_{00})$ band is ~0.0095 $cm^{-1}$. Transitions in the $\Sigma(0_{00}) \leftarrow \Sigma(1_{01})$ band with $J' < 4$ have experimentally limited FWHM of ~0.0029 $cm^{-1}$.

Table 1. Molecular parameters for Ar-$D_2O$ (in $cm^{-1}$). [a]

| | $\Sigma(1_{01}) \leftarrow \Sigma(0_{00})$ | $\Pi(1_{01}) \leftarrow \Sigma(0_{00})$ | $\Sigma(0_{00}) \leftarrow \Sigma(1_{01})$ |
|---|---|---|---|
| $\nu_0$ | 2792.3260(1) | 2803.050(5) | 2780.8906(4) |
| $B'(e)$ | 0.0908000(37) | 0.09487(62) | 0.092808(37) |
| $D'(e)$ | $2.383(28) \times 10^{-6}$ | $0.50(23) \times 10^{-4}$ | $-5.00(90) \times 10^{-6}$ |
| $H'$ | | | $-4.31(57) \times 10^{-8}$ |
| $B'(f)$ | | 0.0925(21) | |
| $D'(f)$ | | $2.4(19) \times 10^{-4}$ | |
| $n$ | 19 | 11 | 18 |
| rmsd | 0.00018 [c] | 0.0066 [d] | 0.00059 |
| $B''$ [b] | 0.093262186 | | 0.09103344 |
| $D''$ [b] | $2.60637 \times 10^{-6}$ | | $1.76655 \times 10^{-6}$ |
| $H''$ [b] | $-8.026 \times 10^{-11}$ | | $-4.5 \times 10^{-10}$ |

[a] Quantities in parentheses are $1\sigma$ from the least-squares fit, in units of the last quoted digit. $n$ is the number of observed lines and rmsd is the root mean square average error in the fit.

[b] Ground state parameters are from Suzuki et al.[4] for $\Sigma(0_{00})$ and from Zwart and Meerts[5] for $\Sigma(1_{01})$.

[c] Two additional lines ($R(8)$ and $R(9)$) were given zero weight; their residuals were 0.0033 and 0.0114 $cm^{-1}$, respectively.

[d] Note that 7 upper state $\Pi(1_{01})$ levels (11 transitions) were fitted with 5 parameters, so the statistics are not very meaningful!

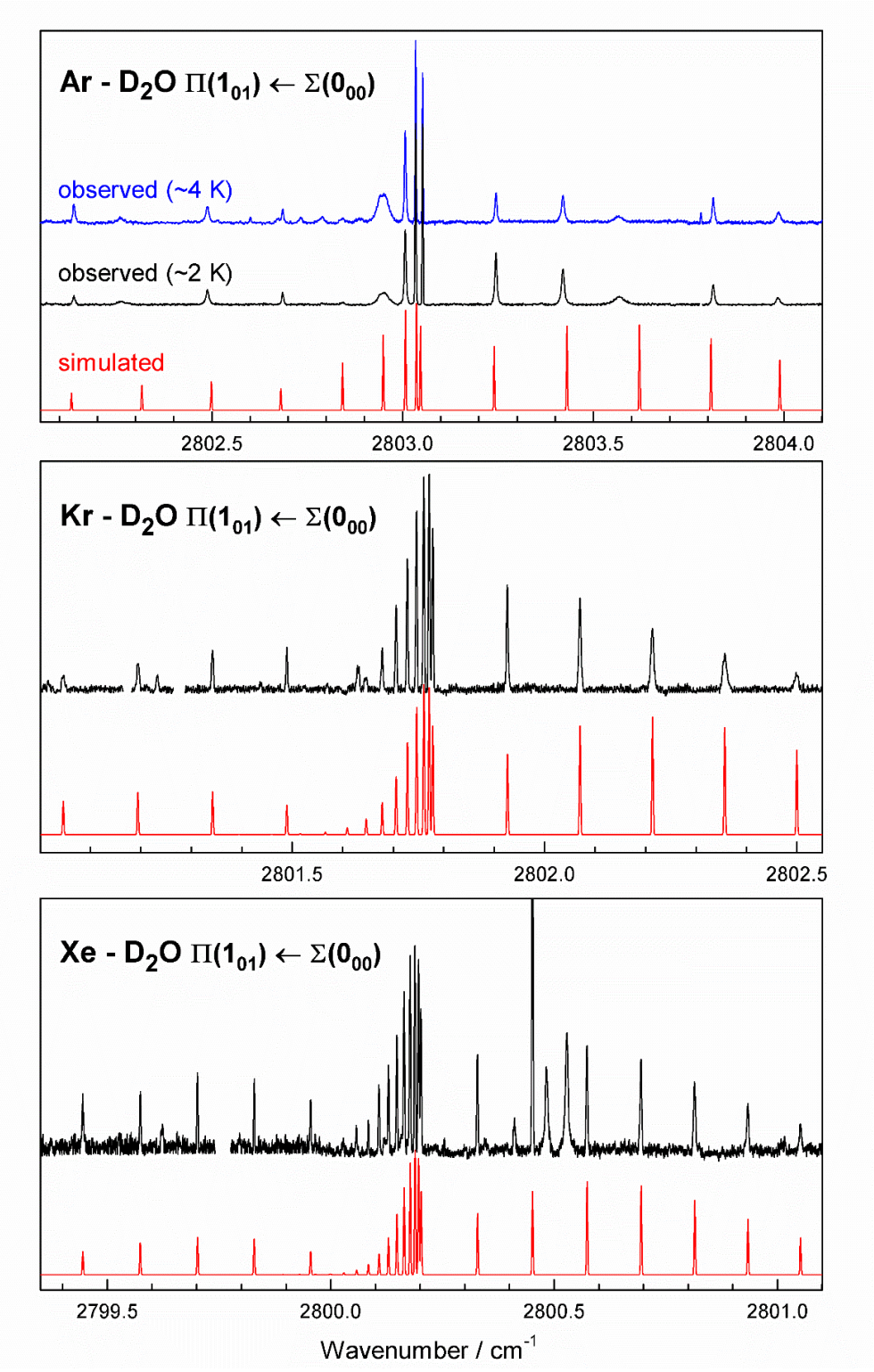


Figure 2. Observed and simulated spectra of the $\Pi(1_{01}) \leftarrow \Sigma(0_{00})$ band of Ar-, Kr-, and Xe-$D_2O$. Gaps in the observed spectra correspond to regions of $D_2O$ absorption.

### 2.2. Kr-$D_2O$

The Kr-$D_2O$ parallel bands are illustrated in Fig. 3 and the perpendicular band in Fig. 2 (central panel); all three spectra correspond to an effective temperature of about 2 K. The $\Pi(1_{01}) \leftarrow \Sigma(0_{00})$ (≈2802 $cm^{-1}$) perpendicular band shows almost no resolved isotopic splitting. Its analysis is straightforward and yields parameters, listed in Table 2, which result in a very satisfactory root mean square deviation (rmsd) of 0.0002 $cm^{-1}$. This good fit stands in contrast to the perturbed nature of the Ar-$D_2O$ $\Pi(1_{01}) \leftarrow \Sigma(0_{00})$ band in the previous section. The widths of the Kr-$D_2O$ transitions increase steadily with increasing $J'$ value, especially in the *P*- and *R*-branches (see Fig. 2). This is partly due to unresolved isotopic splitting, but there seems to be additional lifetime (predissociation) broadening as well.

The $\Sigma(0_{00}) \leftarrow \Sigma(1_{01})$ (≈2780 $cm^{-1}$) band shows some resolved Kr isotopic splitting at higher *J* values, but the $\Sigma(1_{01}) \leftarrow \Sigma(0_{00})$ (≈2791 $cm^{-1}$) band shows large isotopic splitting and perturbation effects for all *J* values. The strongest component in each *P*- and *R*-branch line of this band (see Fig. 3) is due to $^{84}Kr$, the most abundant (57 %) isotope. Note how the *P*(3) and *R*(1) lines are weaker and slightly lower in frequency than expected. Each has a rather obvious satellite line located 0.066 $cm^{-1}$ higher, due to a $J' = 2$ perturbing level. The assignment of these satellites (at 2790.596 and 2791.325 $cm^{-1}$ in Fig. 3) as real *P*(3) and *R*(1) transitions of $^{84}Kr$-$D_2O$ is confirmed by the ground state combination difference. Examining the spectrum further, it is clear that the $\Sigma(1_{01})$ upper state must be perturbed by another state which starts higher in energy for low $J'$, crosses $\Sigma(1_{01})$ just above $J' = 2$ (for $^{84}Kr$-$D_2O$), and then moves lower in energy for $J' = 3$ and higher (the crossing point is different for different Kr isotopes). Thus the perturber has a smaller *B* value and larger isotope splittings than the unperturbed $\Sigma(1_{01})$ state, and these splittings are (partially) transferred to $\Sigma(1_{01})$ by the interaction. The reason for the small *B* value and large isotope splittings is that the perturber necessarily involves highly excited intermolecular vibration mode(s), as discussed further below.

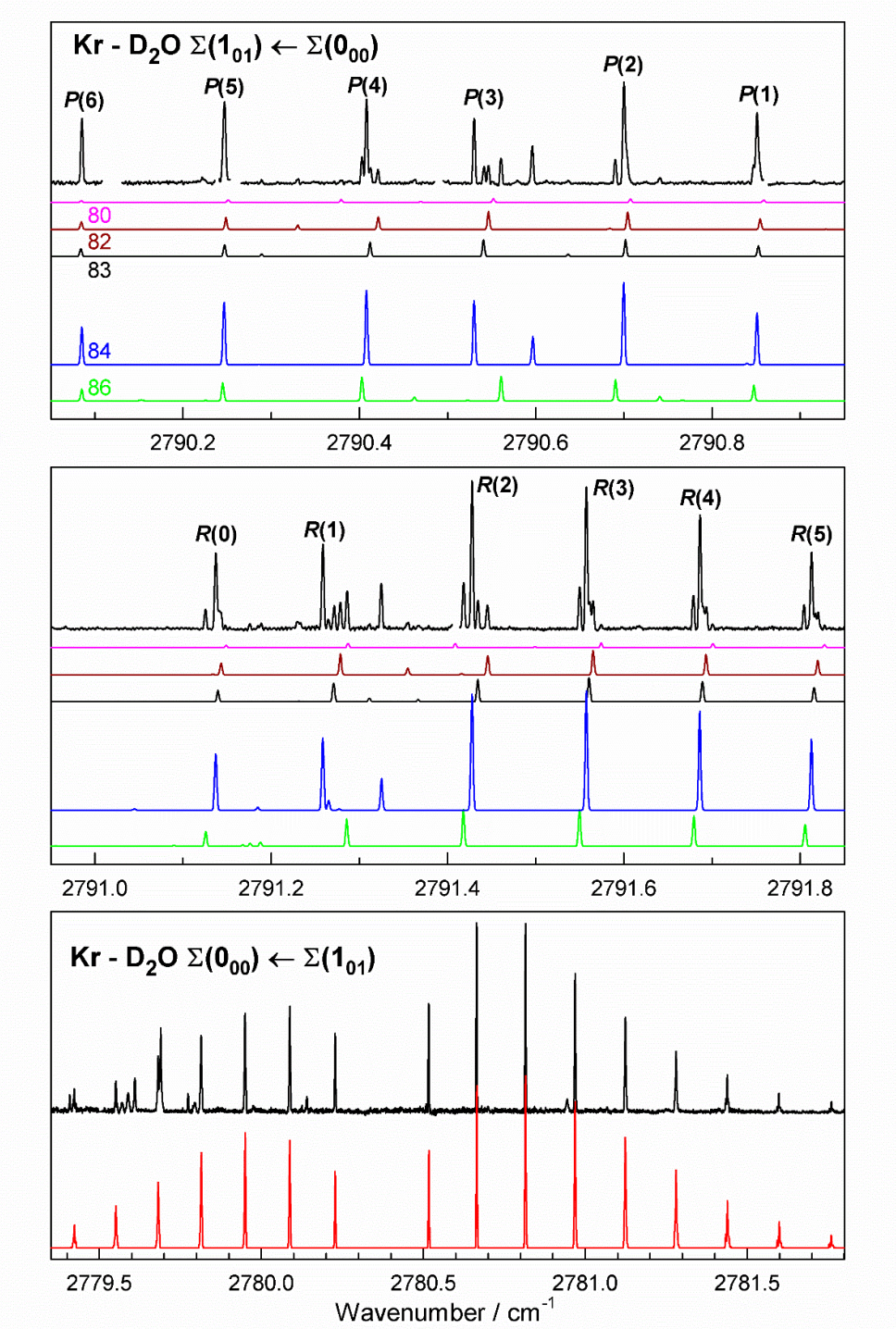


Figure 3. Observed and simulated spectra of Kr-$D_2O$. Gaps in the observed spectra correspond to regions of $D_2O$ and $(D_2O)_2$ absorption. Weaker lines to the low frequency side of the observed spectrum in the bottom panel are $(D_2O)_2$ absorptions.

Table 2. Molecular parameters for Kr-$D_2O$ (in $cm^{-1}$). [a]

| | $\Sigma(1_{01}) \leftarrow \Sigma(0_{00})$ | $\Pi(\text{pert}) \leftarrow \Sigma(0_{00})$ | $\Pi(1_{01}) \leftarrow \Sigma(0_{00})$ | $\Sigma(0_{00}) \leftarrow \Sigma(1_{01})$ |
|---|---|---|---|---|
| $\nu_0$ | 2790.9967(2) | 2791.1863(5) | 2801.7818(2) | 2780.3712(3) |
| $B'(e)$ | 0.0713183(78) | 0.044019(52) | 0.072423(21) | 0.072860(16) |
| $D'(e)$ | $[0.969 \times 10^{-6}]$ | [0.0] | $-2.40(86) \times 10^{-6}$ | $2.80(18) \times 10^{-6}$ |
| $B'(f)$ | | - | 0.0711519(88) | |
| $D'(f)$ | | - | $3.55(19) \times 10^{-6}$ | |
| $B_{adj}'$ | $[-9.733 \times 10^{-5}]$ | $7.65(90) \times 10^{-3}$ | | $[4.129 \times 10^{-5}]$ |
| *Offset* | -0.002022(60) | -0.05407(30) | | -0.00038(11) |
| $W$ | 0.008830(77) | | | |
| $W_{adj}$ | 0.0427(28) | | | |
| $n$ | 51 | | 15 | 24 |
| rmsd | 0.00044 | | 0.00021 | 0.0056 |
| $B''$ | 0.07286304(12) | | | 0.071554384(79) |
| $D''$ | $1.2609(47) \times 10^{-6}$ | | | $0.9694(32) \times 10^{-6}$ |
| $B_{adj}''$ | $4.129(28) \times 10^{-5}$ | | | $-9.733(25) \times 10^{-5}$ |
| $n$ | 16 | | | 14 |
| rmsd | 0.027 MHz | | | 0.017 MHz |

[a] Quantities in parentheses are 1σ from the least-squares fit, in units of the last quoted digit. $n$ is the number of observed lines in a fit, and rmsd the root mean square average error. Quantities in square brackets were held fixed. Units are $cm^{-1}$ except for ground state rmsd (MHz), *Offset* ($cm^{-1}$/Dalton), $B_{adj}$, $W_{adj}$ ([Dalton]$^{-1}$). Origins and rotational parameters refer specifically to $^{84}$Kr-$D_2O$, while $B_{adj}$, $W_{adj}$, and *Offset* describe how these parameters vary with Kr isotope. Ground state parameters, from our unified fit to the microwave data of Van Wijngaarden and Jäger,[12] were held fixed for the infrared fits.

In order to treat the Kr isotope effects in a unified manner we use an approach similar to that used previously for $CO_2$-Kr[17] and $CO_2$-Xe.[18] For the isotopic dependence of the rotational constants $B$ and $D$, we assume:

$$B(N) = B(N_0) \times [F_B(N) + B_{adj} \times (N - N_0)]$$

$$D(N) = D(N_0) \times [F_B(N) + B_{adj} \times (N - N_0)]^2,$$

where N represents the Kr atomic mass number, and $N_0 = 84$, the most abundant isotope. For simplicity, we used atomic mass number rather than the actual atomic mass. $F_B$ is the rigid rotor scaling factor, equal to the inverse ratio of the reduced mass of a particular isotopologue relative to $^{84}$Kr-$D_2O$. $B_{adj}$ is an empirical correction term to allow for departure from exact rigid rotor scaling. Fortunately, precise Kr-$D_2O$ microwave pure rotational data are available from Van Wijngaarden and Jäger,[11] enabling us to test isotope dependence and determine the $B_{adj}$ parameter. The lower part of Table 2 shows parameters from our analysis of their data, with separate fits and different $B_{adj}$ values for the $\Sigma(0_{00})$ and $\Sigma(1_{01})$ ground states of *ortho* and *para* Kr-$D_2O$. The rmsd of our microwave fits are larger than those in the original work,[11] but still quite good (0.027 and 0.017 MHz, respectively). Moreover, note that each of our unified fits involves only three adjustable parameters ($B$, $D$, $B_{adj}$) as compared to eight parameters in Ref. 11 ($B$ and $D$ values for each of 4 isotopes, not counting hyperfine parameters). The main advantage of the unified approach is that the ground state $B_{adj}$ values can now be used for the excited vibrational states in our infrared spectra. Also, the model automatically gives parameters for $^{83}$Kr-$D_2O$, which was not included in the microwave results.[11] The isotopic dependence of a vibrational band origin is modeled by simply assuming a linear dependence on atomic mass number, $\nu_0(N) = \nu_0(N_0) + Offset \times (N - N_0)$. For the present purposes, the results from this relationship are negligibly different from a more realistic model where, for example, a harmonic stretching frequency scales as the square root of a reduced mass.

There are only a few resolved isotopic splittings in the $\Sigma(0_{00}) \leftarrow \Sigma(1_{01})$ ($\approx$2780 cm$^{-1}$) band (lowest panel of Fig. 3), but it is still possible to apply the unified model and the results are listed in the final column of Table 3. For this infrared fit, the ground state parameters are fixed at the values determined in our microwave fit, and the excited state value of $B_{adj}$ is fixed at the ground state value (note that this is the $\Sigma(0_{00})$ value since *para* and *ortho* are interchanged in the (001) upper state). This leaves three adjustable parameters ($B'$, $D'$, and *Offset*) to fit 24 observed transitions with an rmsd of 0.0006 cm$^{-1}$. The resulting value of *Offset* for the $\Sigma(0_{00})$ excited state is small and not very well determined. It implies a band origin shift of only -0.0023 cm$^{-1}$ in going from $^{80}$Kr-$D_2O$ to $^{86}$Kr-$D_2O$.

Successful modelling of the highly perturbed $\Sigma(1_{01}) \leftarrow \Sigma(0_{00})$ ($\approx$2791 cm$^{-1}$) band requires the introduction of a perturbing state with a fairly large *Offset* value and a relatively small $B$

value, both reasonable outcomes as explained below. The nature of the perturbation is illustrated in Fig. 4, which shows how levels of a perturbing state cross those of $\Sigma(1_{01})$ from above, with the crossings occurring between $J = 1$ and 2 for $^{86}$Kr-$D_2O$, between $J = 2$ and 3 for $^{82,83,84}$Kr-$D_2O$, and between $J = 3$ and 4 for $^{80}$Kr-$D_2O$ (for clarity, $^{82}$Kr and $^{83}$Kr are omitted in Fig. 4). The much larger isotopic splittings of the (dark) perturbing state are thus partially transferred to the (bright) $\Sigma(1_{01})$ state. The interaction matrix element connecting $\Sigma(1_{01})$ and the perturber, assumed to be a $\Pi$ state, has the form $W \times 2[J(J+1)/2]^{1/2}$, where $W$ is a Coriolis coupling term. One expects the isotopic variation of $W$ to be similar to that of $B$, and scaling $W$ by $F_B$ does give a reasonable fit, but better results are obtained by introducing an empirical correction parameter $W_{adj}$ analogous to $B_{adj}$, so that $W(N) = W(N_0) \times [F_B(N) + W_{adj} \times (N - N_0)]$. Final results for the $\Sigma(1_{01}) \leftarrow \Sigma(0_{00})$ band are listed in the left-hand columns of Table 2. For this infrared fit, ground state parameters are again fixed at the values from our microwave fit, and the excited state $D$ and $B_{adj}$ parameters for $\Sigma(1_{01})$ are fixed at ground state values. A total of nine parameters are adjusted to fit 54 observed transitions, with a resulting rmsd of about 0.0004 $cm^{-1}$. It is important to note that among these transitions are 39 involving Kr isotopes other than the dominant $^{84}$Kr, and also 11 directly involving the perturber state. The parameters varied include a band origin, $B$ value, and *Offset* parameter for both the $\Sigma(1_{01})$ and $\Pi$(perturber) states, plus the Coriolis parameter, $W$, and its empirical isotopic variation, $W_{adj}$. Finally, there is a separate $B_{adj}$ parameter for the perturber state, the justification being that this state has a very different nature than $\Sigma(0_{00})$ or $\Sigma(1_{01})$ since it involves considerable excitation of large amplitude intermolecular modes. As noted, the analysis utilizes a $\Pi$ state as the perturber. We also tried assuming a $\Sigma$ state perturber, in which case the interaction matrix element is a constant with no rotational dependence (equal to about 0.03 $cm^{-1}$). However, this $\Sigma$ perturber analysis results in a significantly worse fit than the original $\Pi$ perturber analysis.

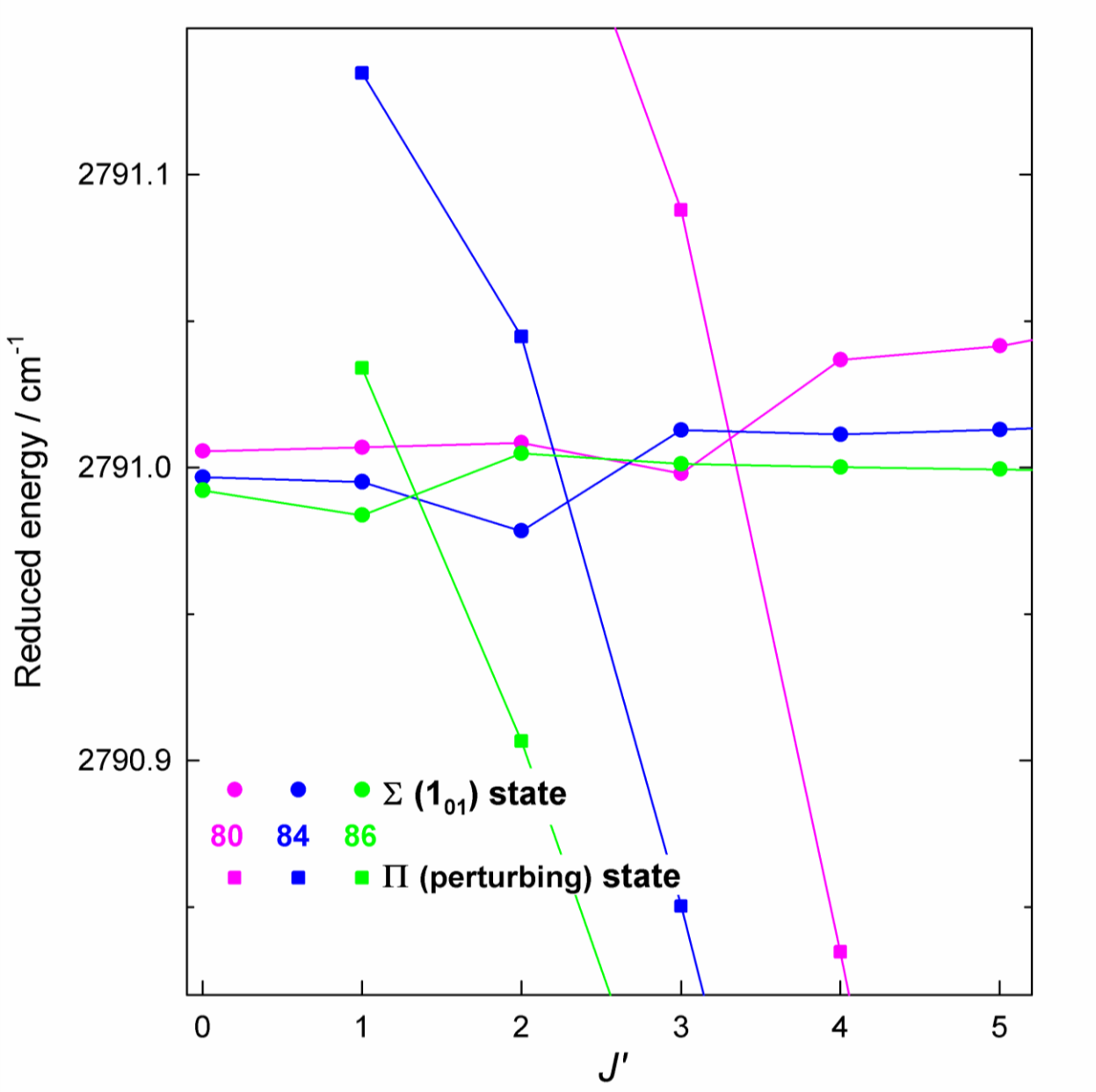


Figure 4. Illustration of the perturbation affecting the excited $\Sigma(1_{01})$ state of Kr-$D_2O$. For clarity, all rotational energies are reduced by the quantity $B_{\text{eff}} \times J(J+1)$, with $B_{\text{eff}} = 0.071$ cm$^{-1}$, and the $^{82}$Kr and $^{83}$Kr isotopologues are omitted. Note how the levels of the $\Sigma(1_{01})$ state (circles) are shifted by interactions with a perturbing $\Pi$ state (squares) which crosses the $\Sigma(1_{01})$ state at different points depending on isotope.

The success of the Kr-$D_2O$ $\Sigma(1_{01}) \leftarrow \Sigma(0_{00})$ (≈2791 $cm^{-1}$) band analysis can be judged from the good agreement of observed and simulated spectra in the upper two panels of Fig. 3. The parameters obtained in the fit deserve some comment. The *B* value of the excited $\Sigma(1_{01})$ state is similar to that of the ground $\Sigma(1_{01})$ state, as expected. The excited $\Sigma(1_{01})$ state *Offset* parameter is small (though larger than that of $\Sigma(0_{00})$ above), and corresponds to a band origin shift of -0.0121 $cm^{-1}$ in going from $^{80}$Kr-$D_2O$ to $^{86}$Kr-$D_2O$. The *B* value obtained for the Π (perturber) state is 0.044 $cm^{-1}$ (for $^{84}$Kr), which at first sight seems impossibly small compared to the usual Kr-$D_2O$ *B* value of about 0.072 $cm^{-1}$. However, the only reasonable perturbing state involves excitation of the $D_2O$ $\nu_1$ intramolecular vibration plus considerable excitation of (floppy) intermolecular vibration(s), and the energy of this intermolecular excitation is approximately 116 $cm^{-1}$, the amount by which $\nu_1$ lies below $\nu_3$. Calculated[13] binding energies of Kr-$D_2O$ are 121 $cm^{-1}$ for $\Sigma(0_{00})$ or 127 $cm^{-1}$ for $\Sigma(1_{01})$, so the perturbing state lies just below the dissociation threshold. The only available Kr-$D_2O$ calculation[13] does not include intermolecular vibrational states this high in energy, but in some other water-Rg calculations there are a number of examples of high lying intermolecular states with greatly reduced effective *B* values.[19,20] So the small *B* value of the perturber state is not unreasonable. The positive value of $B_{adj}$ for the perturber state is sufficiently large and positive that it causes *B* to vary from 0.0431 to 0.0445 $cm^{-1}$ in going from $^{80}$Kr to $^{86}$Kr, a reversal in sign of the expected isotopic dependence. This apparently anomalous variation with reduced mass may not be real, in that it could be a result of the fitting procedure which compensates for imperfections in our model. Or, it could represent a real variation of the effective *B* value due to isotope dependent mixing of the perturber state with other nearby intermolecular vibrations. The perturber state has a relatively large *Offset* value, which is just what we would expect for a highly excited intermolecular vibration: intermolecular modes depend much more strongly on Kr mass than do intramolecular ($D_2O$) vibrations. The *Offset* value represents a band origin shift of -0.3244 $cm^{-1}$ in going from $^{80}$Kr-$D_2O$ to $^{86}$Kr-$D_2O$. The Coriolis interaction parameter, *W*, has a value of 0.0088 $cm^{-1}$ for $^{84}$Kr, and the value determined for $W_{adj}$ means that *W* varies from 0.0074 to 0.0095 $cm^{-1}$ in going from $^{80}$Kr to $^{86}$Kr.

### 2.3. Xe-$D_2O$

The $\Sigma(0_{00}) \leftarrow \Sigma(1_{01})$ (≈2779 $cm^{-1}$) and $\Sigma(1_{01}) \leftarrow \Sigma(0_{00})$ (≈2790 $cm^{-1}$) parallel bands of Xe-$D_2O$ are illustrated in Fig. 5 and the $\Pi(1_{01}) \leftarrow \Sigma(0_{00})$ (≈2800 $cm^{-1}$) perpendicular band in Fig. 2 (lower panel). The quality of these observed spectra is significantly worse than those of Ar- and Kr-$D_2O$, even though we tried to use similar gas mixtures. The Xe-$D_2O$ spectra have much more interference from transitions due to the $D_2O$ monomer and dimer (the spectrum of $(D_2O)_2$ in this region is reported in Ref. 15).

The 2779 and 2800 $cm^{-1}$ band structures are clearly evident and have no resolved isotopic splitting or large perturbations. In contrast, the 2790 $cm^{-1}$ band (upper panel, Fig. 5) appears to be fragmented into many weak lines, similar to (but worse than) its Kr-$D_2O$ counterpart (upper panel, Fig. 3). The fragmentation of this band is doubtless due to similar interactions with dark background states involving highly excited intermolecular modes, and we initially hoped to analyze the perturbation in detail, as with Kr-$D_2O$. This unfortunately turned out to be impossible, but as a first step in the attempt, we made a unified fit of the ground vibrational state based on the microwave results of Wen and Jäger.[12] Details of this fit are entirely analogous to those of Kr-$D_2O$, and the results are shown at the bottom of Table 3 (the standard Xe atomic mass number is taken as $N_0 = 131$). From the microwave fit, we have precise ground state combination differences for each isotopologue of Xe-$D_2O$ which in principle could allow us to assign transitions in the 2790 $cm^{-1}$ band even without recognizing the band structure. For example, the difference between the $R(0)$ and $P(2)$ lines in the infrared spectrum must equal the difference between the ground state $J'' = 0$ and 2 rotational levels, which is 0.3747, 0.3739, 0.3736, 0.3729, and 0.3721 $cm^{-1}$ for $^{129}$Xe-, $^{131}$Xe-, $^{132}$Xe-, $^{134}$Xe-, and $^{136}$Xe-$D_2O$, respectively. Assuming, as we suspect, that the $\Sigma(1_{01}) \leftarrow \Sigma(0_{00})$ band origin is around 2789.68 $cm^{-1}$, we observe sets of four lines each in the expected $R(0)$ and $P(2)$ regions whose differences equal 0.3743, 0.3727, 0.3739, and 0.3741 $cm^{-1}$. This looks promising, and when we examine other line pairs ($R(1)$ and $P(3)$, etc.) we also find possible matches. Many of these could be correct assignments, but putting them all together in a coherent pattern proves impossible! Our conclusion is that the $\Sigma(1_{01})$ excited state experiences strong perturbations which are probably due to more than one highly excited intermolecular vibration (at ≈116 $cm^{-1}$) within the manifold built on the $D_2O$ $\nu_1$ intramolecular vibration. The calculated binding energy of Xe-$H_2O$ is 140

$cm^{-1}$, and that of Xe-$D_2O$ is likely to be around 138 $cm^{-1}$ (based on the difference between Kr-$D_2O$ and Kr-$H_2O$).[13,20]

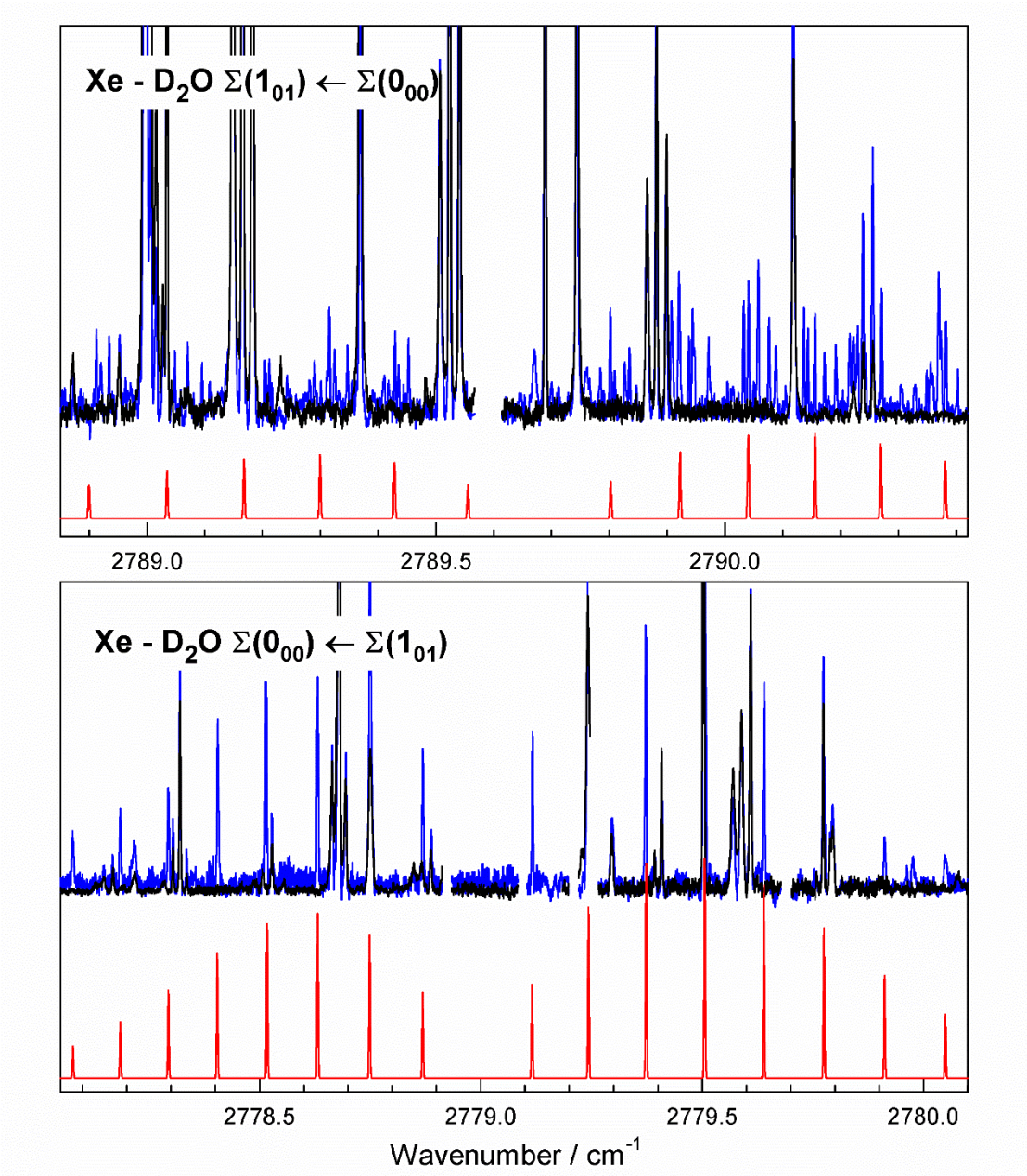


Figure 5. Observed and simulated spectra of Xe-$D_2O$ parallel bands. The Xe-$D_2O$ transitions (Xe/$D_2O$/He spectrum shown in blue) are strongly overlapped by $(D_2O)_2$ transitions[15] ($D_2O$/He spectrum in black). The 2779 $cm^{-1}$ band is well represented by the simulated spectrum, shown in red, but the 2790 $cm^{-1}$ band is highly perturbed and is not rotationally assigned, so its exact band origin is uncertain (the simulated spectrum is an approximate guess).

Table 3. Molecular parameters for Xe-$D_2O$ (in $cm^{-1}$). [a]

| | $\Sigma(1_{01}) \leftarrow \Sigma(0_{00})$ | $\Pi(1_{01}) \leftarrow \Sigma(0_{00})$ | $\Sigma(0_{00}) \leftarrow \Sigma(1_{01})$ |
|---|---|---|---|
| $\nu_0$ | 2789.68 [b] | 2800.2051(3) | 2778.9909(5) |
| $B'(e)$ | | 0.061913(13) | 0.062526(40) |
| $D'(e)$ | | $1.28(30) \times 10^{-6}$ | $3.26(57) \times 10^{-6}$ |
| $B'(f)$ | | 0.0609638(34) | |
| $D'(f)$ | | $0.528(47) \times 10^{-6}$ | |
| $n$ | | 20 | 12 |
| rmsd | | 0.00027 | 0.00076 |
| $B''$ | 0.062328884(75) | | 0.061209973(79) |
| $D''$ | $0.7988(29) \times 10^{-6}$ | | $0.5854(30) \times 10^{-6}$ |
| $B_{adj}''$ | $0.1359(18) \times 10^{-4}$ | | $0.3366(19) \times 10^{-4}$ |
| $n$ | 20 | | 17 |
| rmsd | 0.014 MHz | | 0.023 MHz |

[a] Quantities in parentheses are 1σ from the least-squares fit, in units of the last quoted digit. n is the number of observed lines in a fit, and rmsd the root mean square average error. Units are $cm^{-1}$ except for ground state rmsd (MHz) and $B_{adj}$ ($[Dalton]^{-1}$). Ground state rotational parameters refer specifically to $^{131}Xe$-$D_2O$, while $B_{adj}$ describes the variation with Xe isotope. Ground state parameters, from our unified fit to the microwave data of Wen and Jäger,[12] were held fixed for the infrared fits.

Returning to the $\Sigma(0_{00}) \leftarrow \Sigma(1_{01})$ (≈2779 $cm^{-1}$) and $\Pi(1_{01}) \leftarrow \Sigma(0_{00})$ (≈2800 $cm^{-1}$) bands of Xe-$D_2O$, they are analyzed by fixing the ground state parameters at the values from our microwave fits, with results as shown in Table 3. For the $\Pi(1_{01}) \leftarrow \Sigma(0_{00})$ band, five parameters are varied to fit 20 observed transitions with a very good rmsd of 0.0003 $cm^{-1}$. For the $\Sigma(0_{00}) \leftarrow \Sigma(1_{01})$ band, three parameters are varied to fit 12 observed transitions with an rmsd of 0.0008 $cm^{-1}$, and this larger deviation appears to be due to the poor quality of the spectrum and not due to obvious upper state perturbations.

### 2.4. Line broadening

The observed line broadening in the $\Sigma(0_{00}) \leftarrow \Sigma(1_{01})$ and $\Pi(1_{01}) \leftarrow \Sigma(0_{00})$ bands of Kr- and Xe-$D_2O$ is at least partly due to unresolved isotopic splitting, and this makes it difficult to

measure reliably the possible effects due to lifetime broadening (predissociation). No isotopic splitting has to be considered for Ar-$D_2O$, for which observed broadening effects are summarized in Table 4 and Fig. 6. The broadening of the rotational levels of the $\Sigma(0_{00})$ upper state is smaller than we can measure up to $J' = 3$, reaches a maximum of about 0.0096 $cm^{-1}$ at $J' = 8$, and then declines somewhat up to the last observed level, $J' = 12$. In contrast, broadening in the $\Sigma(1_{01})$ upper state is already present for $J' = 0$, with a value which is roughly constant (≈0.009 $cm^{-1}$) up to $J' = 6$. It then rises to a peak of 0.02 $cm^{-1}$ at $J' = 10$, and falls back to about 0.005 $cm^{-1}$ at $J' = 11$. Finally, the $\Pi(1_{01})$ upper state has highly variable widths, including rather large ones for the $J' = 3(e)$ component (0.04 $cm^{-1}$, *P*- and *R*-branches) and $J' = 4(f)$ component (0.03 $cm^{-1}$, *Q*-branch). Calculated[10] binding energies for Ar-$D_2O$ are about 95 $cm^{-1}$ for $\Sigma(0_{00})$, 102 $cm^{-1}$ for $\Sigma(1_{01})$, and 91 $cm^{-1}$ for $\Pi(1_{01})$, and in isolated $D_2O$ the $\nu_1$ vibrational state lies 116 $cm^{-1}$ below the $\nu_3$ state. Thus the Ar-$D_2O$ states associated with $\nu_1$ which could perturb (and dissociate) the present $\nu_3$ spectra lie roughly 10 to 25 $cm^{-1}$ above the $\nu_1$ dissociation threshold. Of course $\nu_3$ is much further above the thresholds for $2\nu_2$ (≈350 $cm^{-1}$), $\nu_2$ (≈1500 $cm^{-1}$), and the ground state (≈2700 $cm^{-1}$). Binding energies for Kr- and Xe-$D_2O$ are larger than those of Ar-$D_2O$ by roughly 25 and 40 $cm^{-1}$, respectively, so their $\nu_3$ upper states probably lie below the $\nu_1$ dissociation threshold. This helps to explain why significant broadening is observed for Ar-$D_2O$, but not Kr- and Xe-$D_2O$.

Perturbations and broadening in the analogous $\nu_3$ spectra of Ar-$H_2O$ were studied by Nesbitt and Lascola,[21,22] with further theoretical analysis reported by Bissonette and Clary.[23] It was observed that transitions remained sharp in the $\Sigma(1_{01}) \leftarrow \Sigma(0_{00})$ and $\Sigma(0_{00}) \leftarrow \Sigma(1_{01})$ bands, and in the *Q*-branch of the $\Pi(1_{01}) \leftarrow \Sigma(0_{00})$ band, but were broadened by predissociation in the *P*- and *R*-branches of the $\Pi(1_{01}) \leftarrow \Sigma(0_{00})$ band. The *Q*-branch accesses the *f* symmetry components of the $\Pi(1_{01})$ state, while the *P*- and *R*-branches access the *e* components. The fact that the $\nu_3$ $\Pi(1_{01})$ levels with *e* symmetry are broadened, but not the *f* levels, was nicely explained as being due to the energies of the respective symmetry-allowed interaction channels being above or below the $\nu_1$ dissociation threshold. In the present case, Ar-$D_2O$ binding energies are slightly increased (≈5 $cm^{-1}$) compared to Ar-$H_2O$, but, more significantly, the separation between $\nu_3$ and $\nu_1$ is larger for $D_2O$ (116 $cm^{-1}$) than for $H_2O$ (99 $cm^{-1}$). The combined effect is that the Ar-$D_2O$ $\nu_3$ $\Pi(1_{01})$ *e* and *f* components both lie above their respective $\nu_1$ dissociation

thresholds, as do the $\nu_3$ $\Sigma(0_{00})$ and $\Sigma(1_{01})$ states. Thus all our observed bands show some broadening, which is almost certainly due to interactions with levels just above the $\nu_1$ threshold. Unfortunately, it is not currently possible to make a detailed analysis of these effects for Ar-$D_2O$ similar to that of Nesbitt and Lascola[22] for Ar-$H_2O$. This is partly because we do not have detailed calculations of high-lying (above dissociation) Ar-$D_2O$ energy levels, but also because our low rotational temperatures (compared to Nesbitt and Lascola) mean that fewer lines are observed and analysis of the bands is limited, especially for $\Pi(1_{01}) \leftarrow \Sigma(0_{00})$.

Table 4. Lorentzian widths and excited state lifetimes of Ar-$D_2O$ in the (001) state of $D_2O$.

| $J'$ | $\Sigma(0_{00})$ state | | $\Sigma(1_{01})$ state | | $\Pi(1_{01})$ *e* state | | $\Pi(1_{01})$ *f* state | |
|---|---|---|---|---|---|---|---|---|
| | width / $cm^{-1}$ | lifetime / ns | width / $cm^{1}$ | lifetime / ns | width / $cm^{-1}$ | lifetime / ns | width / $cm^{-1}$ | lifetime / ns |
| 0 | <0.0005 | >11 | 0.0074 | 0.72 | | | | |
| 1 | <0.0005 | >11 | 0.0088 | 0.61 | 0.0045 | 1.2 | <0.0005 | >11 |
| 2 | <0.0005 | >11 | 0.0087 | 0.61 | 0.0077 | 0.69 | 0.0006 | 9 |
| 3 | <0.0005 | >11 | 0.0091 | 0.58 | 0.040 | 0.13 | 0.0035 | 1.5 |
| 4 | 0.0011 | 4.8 | 0.0089 | 0.59 | 0.0062 | 0.86 | 0.031 | 0.17 |
| 5 | 0.0006 | 9.5 | 0.0092 | 0.58 | 0.011 | 0.48 | | |
| 6 | 0.0017 | 3.1 | 0.0088 | 0.61 | | | | |
| 7 | 0.0031 | 1.7 | 0.010 | 0.52 | | | | |
| 8 | 0.0096 | 0.55 | 0.012 | 0.45 | | | | |
| 9 | 0.007 | 0.8 | 0.013 | 0.42 | | | | |
| 10 | 0.008 | 0.7 | 0.021 | 0.25 | | | | |
| 11 | (0.005) | (1) | 0.0054 | 0.98 | | | | |
| 12 | (0.003) | (2) | | | | | | |

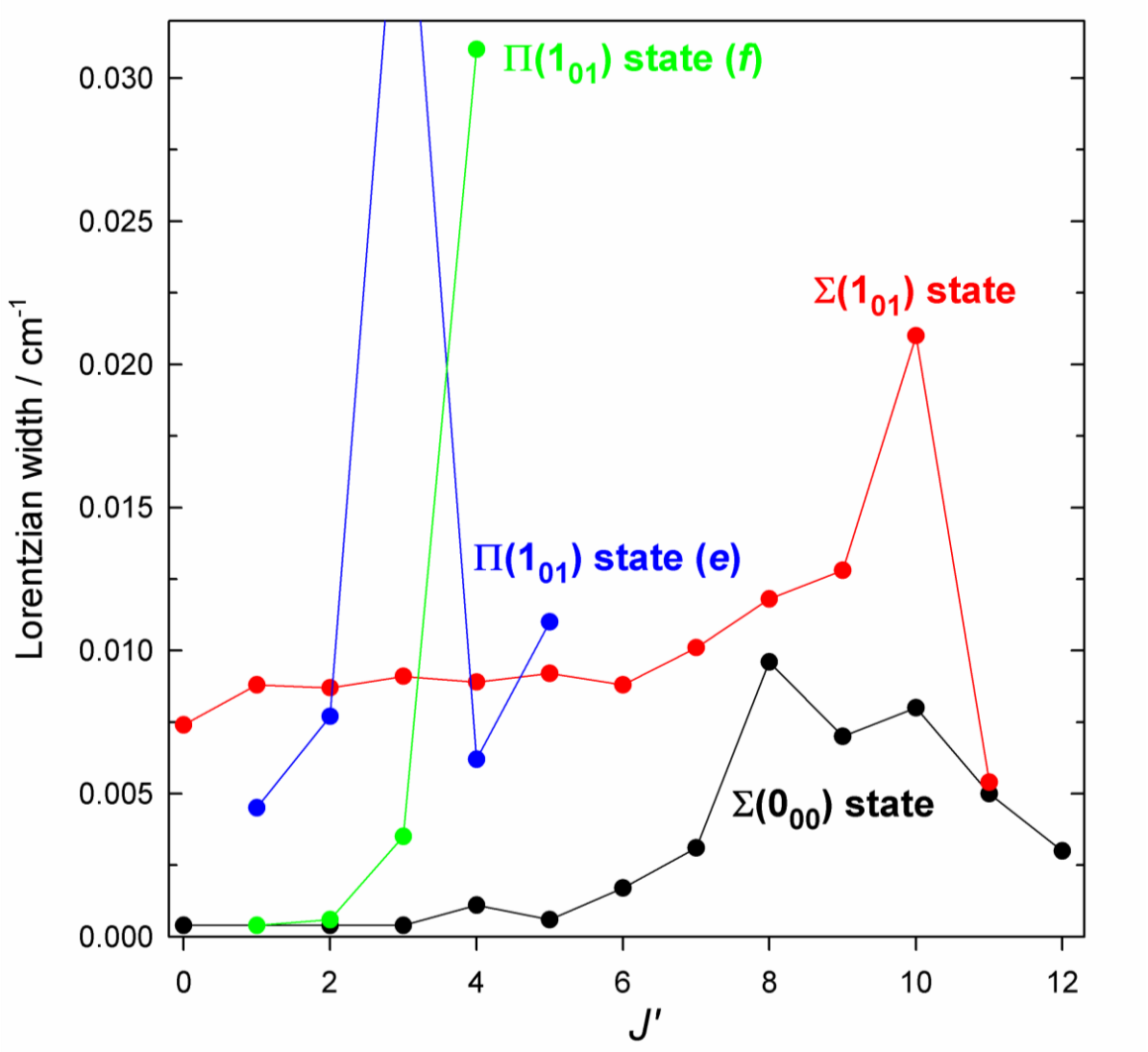


Figure 6. Observed line widths (FWHM) in the spectrum of Ar-$D_2O$. These are the widths, assumed to be Lorentzian in shape, which are in excess of the normal instrumental width (approximately Gaussian in shape) of about 0.0029 $cm^{-1}$.

### 2.5. Vibrational shifts

Vibrational frequency shifts of simple van der Waals dimers containing Rg atoms are often roughly proportional to the Rg polarizability.[24] In Fig. 7, we plot the present Rg-$D_2O$ band origins in this way, showing how they correlate with the respective $0_{00} \leftarrow 1_{01}$ and $1_{01} \leftarrow 0_{00}$ transitions in the $D_2O$ monomer $\nu_3$ band. The fairly large changes indicated by the solid lines connecting $D_2O$ and Ar-$D_2O$ in this plot demonstrate that the rotation of $D_2O$ is significantly

hindered by the nearby Ar atom. But interestingly the degree of hindering then does not change very much in going to Kr and Xe, possibly because their stronger interactions with $D_2O$ are compensated by larger intermolecular distances. The dashed line in Fig. 7 represents the energy of the $J' = 0$ level in each case, in other words the actual band origin. This line, which better represents the purely vibrational shift effect, is indeed approximately linear as a function of polarizability.

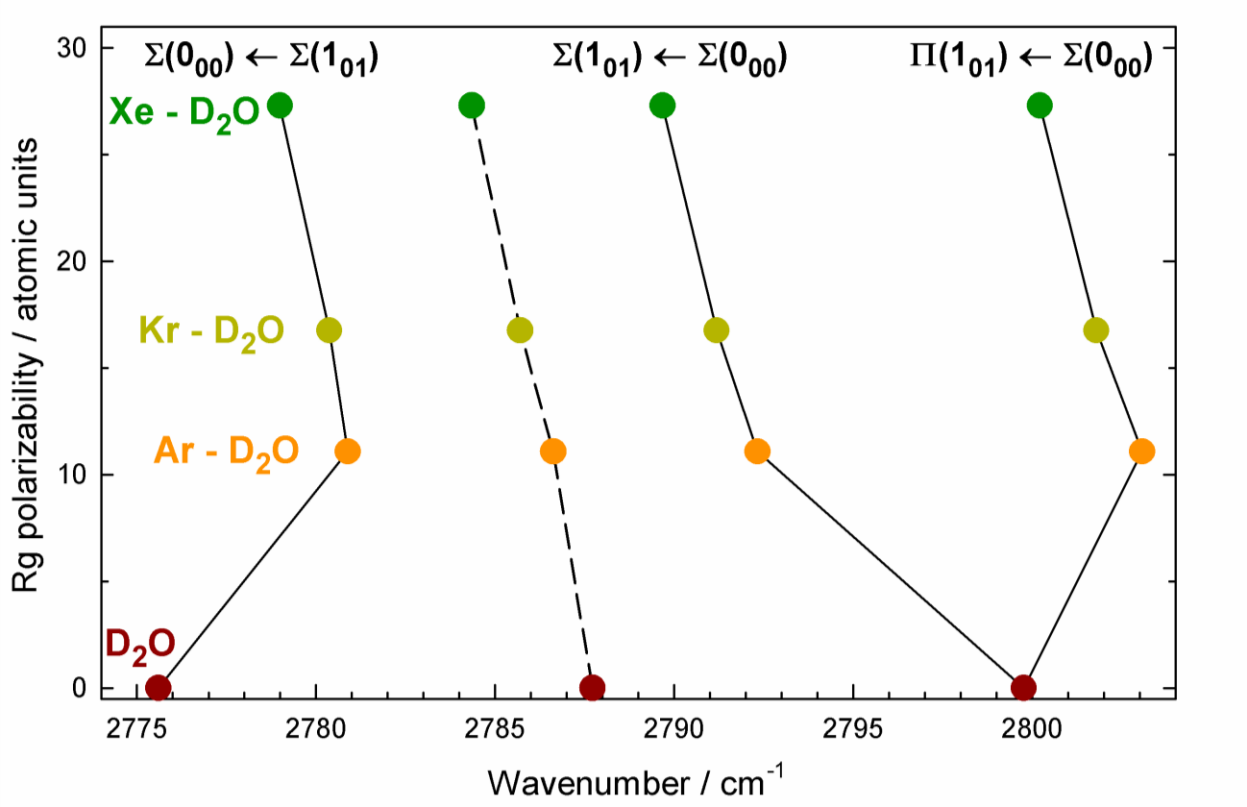


Figure 7. Vibrational frequencies of Rg-$D_2O$ complexes as a function of Rg polarizability. The $D_2O$ monomer $\nu_3$ band $0_{00} \leftarrow 1_{01}$ and $1_{01} \leftarrow 0_{00}$ rotational transitions (*para* and *ortho* spin species, respectively) correlate with the observed Rg-$D_2O$ bands as indicated (solid lines). The energies of the excited state $0_{00}$ levels (that is, the overall band origins) are shown by the dashed line, where we assume that the ratio of the $1_{01}$ level energies in the ground and excited states for $D_2O$-Rg is the same as for $D_2O$.

## 3. Conclusions

Spectra of Rg-$D_2O$ dimers (Rg = Ar, Ke, Xe) in the region of the $D_2O$ $\nu_3$ asymmetric stretch fundamental (≈2800 $cm^{-1}$) have been studied, using a tunable optical parametric oscillator source to probe a pulsed slit jet supersonic expansion. In spite of considerable recent interest in rare gas - water dimers, this represents the first infrared study involving Xe, and one of only a few involving Kr. Three bands were observed for each dimer, labeled as $\Sigma(1_{01}) \leftarrow \Sigma(0_{00})$, $\Pi(1_{01}) \leftarrow \Sigma(0_{00})$, and $\Sigma(0_{00}) \leftarrow \Sigma(1_{01})$. For Ar-$D_2O$, various effects of line broadening due to predissociation (finite lifetime) were observed, particularly for the $\Sigma(1_{01})$ and $\Pi(1_{01})$ upper states. For Kr-$D_2O$, the $\Sigma(1_{01}) \leftarrow \Sigma(0_{00})$ band was notable because it showed large Kr isotope dependent splitting effects due to perturbation by a "dark" background state which could be analyzed in detail. For Xe-$D_2O$, the observed spectra were relatively weak and the $\Sigma(1_{01}) \leftarrow \Sigma(0_{00})$ band was so perturbed as to defy analysis, but the other bands still gave clear results.

## Supplementary Material

Supplementary Material includes tables giving observed and fitted line positions for Ar-, Kr-, and Xe-$D_2O$, and detailed isotopic dependence of molecular parameters for $D_2O$-Kr.

## Acknowledgements

The financial support of the Natural Sciences and Engineering Research Council of Canada is gratefully acknowledged. C.L. and R.G. acknowledge the financial support of the FNRS through CDRs J.0129.20 and J.0113.23 and of the Fédération Wallonie-Bruxelles through the Action de Recherches Concertées (Grant No. ARC iBEAM-18/23-090). R.G. is a FRIA grantee of the Fonds de la Recherche Scientifique (FNRS).

**References**

[1] R. C. Cohen, K. L. Busarow, K. B. Laughlin, G. A. Blake, M. Havenith, Y. T. Lee, and R. J. Saykally, Tunable far infrared laser spectroscopy of van der Waals bonds: Vibration–rotation– tunneling spectra of Ar–$H_2O$, J. Chem. Phys. **89**, 4494-4504 (1988).

[2] J. Makarewicz, Ab initio intermolecular potential energy surfaces of the water-rare gas atom complexes, J. Chem. Phys. **129**, 184310 (2008).

[3] G. T. Fraser, F. J. Lovas, R. D. Suenram, and K. Matsumura, Microwave spectrum of Ar-$H_2O$: Dipole moment, isotopic studies, and $^{17}O$ quadrupole coupling constants, J. Mol. Spectrosc. **144**, 97-112 (1990).

[4] S. Suzuki, R. E. Bumgarner, P. A. Stockman, P. G. Green, and G. A. Blake, Tunable far-infrared laser spectroscopy of deuterated isotopomers of Ar–$H_2O$, J. Chem. Phys. **94**, 824 (1991).

[5] E. Zwart and W. L. Meerts, The submillimeter rotation-tunneling spectrum of Ar-$D_2O$ and Ar-$NH_3$, Chem. Phys. **151**, 407-418 (1991).

[6] S. Li, R. Zheng, Y. Zhu, and C. Duan, Rovibrational spectra of the Ar-$D_2O$ and Kr-$D_2O$ van der Waals complexes in the $\nu_2$ bend region of $D_2O$, J. Mol. Spectrosc. **272**, 27-31 (2012).

[7] J. T. Stewart and B. J. McCall, Additional bands of the Ar–$D_2O$ intramolecular bending mode observed using a quantum cascade laser, J. Mol. Spectrosc. **282**, 34-38 (2012).

[8] L. Xiang, L. Yun, Z. Tian-Xin, and D. Chuan-Xi, New rovibrational subbands of Ar-$D_2O$ complex in the $D_2O$ bending mode region, Acta Physica Sinica **72**, 013401 (2023). doi: 10.7498/aps.72.20221728

[9] K. Didriche and T. Földes, High resolution spectroscopy of the Ar-$D_2O$ and Ar-HDO molecular complexes in the near-infrared range, J. Chem. Phys. **138**, 104307 (2013).

[10] S. Wang, S. He, L. Dai, E. Feng, and W. Huang, A four-dimensional potential energy surface for the Ar–$D_2O$ van der Waals complex: Bending normal coordinate dependence, J. Chem. Phys. **142**, 224307 (2015).

[11] J. Van Wijngaarden and W. Jäger, Rotational spectra of the Kr-$H_2O$ van der Waals complex, Mol. Phys. **98**, 1575-1588 (2000).

[12] Q. Wen and W. Jäger, Rotational Spectroscopic and ab initio Studies of the Xe-$H_2O$ van der Waals Dimer, J. Phys. Chem. A **110**, 7560-7567 (2006).

[13] Z. Wang, E. Feng, C. Zhang, and C. Sun, A new potential energy surface and microwave and infrared spectra of the Kr–$D_2O$ complex, Chem. Phys. Lett. **685**, 9-15 (2017).

[14] N. Moazzen-Ahmadi and A. R. W. McKellar, Spectroscopy of dimers, trimers, and larger clusters of linear molecules, Int. Rev. Phys. Chem. **32**, 611-650 (2013).

[15] A. J. Barclay, A. R. W. McKellar, and N. Moazzen-Ahmadi, Spectra of the $D_2O$ dimer in the O-D fundamental stretch region: vibrational dependence of tunneling splittings and lifetimes, J. Chem. Phys. **150**, 164307 (2019).

[16] C. M. Western, PGOPHER, a program for simulating rotational structure version 8.0, 2014, University of Bristol Research Data Repository, doi:10.5523/bris.huflggvpcuc1zvliqed497r2

[17] T. Gartner, S. Ghebretnsae, A. R. W. McKellar, and N. Moazzen-Ahmadi, Infrared spectra of $CO_2$ – Kr: intermolecular bend and symmetry breaking of the $CO_2$ bend, Chemistry Select **7**, e202202601 (2022).

[18] A. J. Barclay, A. R. W. McKellar, C. M. Western, and N. Moazzen-Ahmadi, New infrared spectra of $CO_2$ – Xe: modeling Xe isotope effects, intermolecular bend and stretch, and symmetry breaking of the $CO_2$ bend, Mol. Phys. **119,** e1919325 (2021); https://doi.org/10.1080/00268976.2021.1919325.

[19] J. Lei, Y. Zhou, D. Xie, and H. Zhu, A new ab initio intermolecular potential energy surface and predicted rotational spectra of the Kr−$H_2O$ complex, J. Chem. Phys. **137**, 224314 (2012).

[20] D. Hou, Y.-T. Ma, X.-L. Zhang, and H. Li, The origins of intra- and inter-molecular vibrational couplings: A case study of $H_2O$-Ar on full and reduced-dimensional potential energy surface, J. Chem. Phys. **144**, 014301 (2016).

[21] D. J. Nesbitt and R. Lascola, Slit-jet near-infrared spectroscopy and internal rotor dynamics of the Ar$H_2O$ van der Waals complex: An angular potential-energy surface for internal $H_2O$ rotation, J. Chem. Phys. **95**, 7917 (1991).

[22] D. J. Nesbitt and R. Lascola, Vibration, rotation, and parity specific predissociation dynamics in asymmetric OH stretch excited $ArH_2O$: A half collision study of resonant V-V energy transfer in a weakly bound complex, J. Chem. Phys. **97**, 8096-8110 (1992).

[23] C. Bissonnette and D. C. Clary, Vibrational predissociation of $ArH_2O$, J. Chem. Phys. **97**, 8111 (1992).

[24] A.J. Barclay, A.R.W. McKellar, and N. Moazzen-Ahmadi, Infrared spectra of $(CO_2)_2$ - Rg trimers, Rg = Ne, Ar, Kr, and Xe, J. Mol. Spectrosc. **387**, 111673 (2022).